IEEE Access
Multidisciplinary | Rapid Review | Open Access Journal

SPECIAL SECTION ON SPECIAL SECTION ON ROADMAP TO 5G ON RISING TO THE CHALLENGE

Received November 22, 2018, accepted December 13, 2018, date of publication December 20, 2018,
date of current version January 11, 2019.

Digital Object Identifier 10.1109/ACCESS.2018.2888981

Spherical Coverage Characterization of 5G Millimeter Wave User Equipment With 3GPP Specifications

KUN ZHAO[1,2], SHUAI ZHANG[2], (Senior Member, IEEE), ZULEITA HO[1], (Member, IEEE), OLOF ZANDER[1], THOMAS BOLIN[1], ZHINONG YING[1], (Senior Member, IEEE), AND GERT FRØLUND PEDERSEN[2], (Senior Member, IEEE)

[1]Radio Access Lab, Sony Mobile Communications AB, 22188 Lund, Sweden
[2]Antennas, Propagation and Millimeter-Wave Systems Section, Department of Electronic Systems, Aalborg University, 9220 Aalborg, Denmark

Corresponding author: Shuai Zhang (sz@es.aau.dk)

This work was supported in part by the Innovationsfonden Project of RANGE and in part by the AAU Young Talent Program.

ABSTRACT Millimeter-wave (mmWave) frequency bands are promising candidate spectrum for the fifth-generation (5G) mobile communication system, but it requires high directional antenna systems to be applied to the base station and the user equipment (UE) for compensating the high path loss. Due to the randomness of mobile wireless channels, antenna systems in a mobile UE must own a large spherical coverage, which raises new challenges for the performance characterization of 5G mmWave UEs. In the latest specification of the Third-Generation Partnership Project (3GPP), the requirement on UE's spherical coverage in mmWave frequencies is defined, which is evaluated with the cumulative distribution function of the effective isotropic radiated power. In this paper, the spherical coverage of mmWave UEs is characterized based on the specification of 3GPP, where the impact of device integration, antenna topologies, and user body blockage on the spherical coverage of UE will be analyzed with simulation and measurement results.

INDEX TERMS Antenna arrays, beam steering, coverage efficiency, mobile handsets, mobile user equipment, spherical coverage, EIRP, CDF, 5G mobile communication.

I. INTRODUCTION

The global shortage of frequency spectrum for cellular communications motivates people to move their attention to mmWave frequency bands, where vast continuous spectrum is available for deploying the new generation mobile network [1]. In the latest and also the first 3GPP 5G specification (Release 15), four frequency bands in the frequency range 2 (FR2) have been arranged for the 5G new radio (NR) [2] (see Table. 1). However, moving up into such a high-frequency range will bring an unfavorable propagation environment for mobile comminutions, such as an increased free space path loss and a higher diffraction loss [3]. A possible solution to overcome the higher propagation loss is to use high gain antenna systems, e.g., antenna arrays, in both BS and UE at mmWave frequency bands [4].

Since a high gain antenna system will naturally narrow the beamwidth of the radiation pattern, antenna systems in a mobile UE must be able to offer a large scanning angle in order to steer the beam towards to an optimal transmitting-receiving angle in a randomly changed mobile channel (see Fig. 1). The range of solid angles that a UE can cover is known as the spherical coverage. Ideally, antenna systems in a mobile handset are preferable to have an isotropic spherical coverage. However, physical limitations and design constraints restrict the maximum spherical coverage that a mobile handset can achieve. Different mmWave antenna arrays have been proposed for the 5G mobile handset in order to resolve this issue [5]–[15]. In [5] and [6], the proposed antenna system can achieve a quasi-isotropic spherical coverage by placing multiple arrays in a mobile handset. The designs of three-dimensional (3D) switchable antenna array are introduced in [8] and [9] to enlarge the spherical coverage.

TABLE 1. NR operating bands in FR2 [2].

NR Operating Band	Frequency
n257	26500 MHz – 29500 MHz
n258	24250 MHz – 27500 MHz
n260	37000 MHz – 40000 MHz
n261	27500 MHz – 28350 MHz

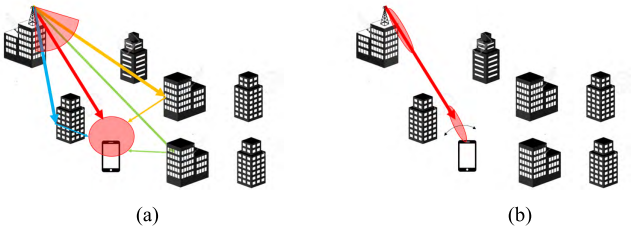

FIGURE 1. Illustration of the cellular propagation channel (a) in a sub-6 GHz frequency band with an omnidirectional antenna in the UE and (b) in a mmWave frequency band with a beam steering antenna system in the UE.

A hybrid antenna module concept is introduced in [10] for the 5G mobile handset, and beam switch antenna designs are introduced in [12] and [13] to realize beam steering over large solid angles.

In addition to antenna designs, the characterization of UE's spherical coverage is also a critical challenge for 5G communication, as the figure of merits used for 3G and 4G communications are not capable for this purpose. Conventionally, network operators set minimum specifications for the over-the-air (OTA) performance of UEs at sub-6 GHz cellular bands, which includes the total radiated power (TRP) and the total isotropic sensitivity (TIS). However, TRP or TIS is not suitable to characterize the beam steering capability of a UE. Parameters that can measure the power radiated towards a specific direction is needed to characterize the spherical coverage of a UE.

In [16], the coverage efficiency and the total scan pattern are defined to measure the spherical coverage of a beam steering antenna system. The total scan pattern can be obtained from all possible beam steering radiation patterns by extracting the best achievable gain at every solid angular point. The total covered solid angles of the antenna system can be retrieved from its total scan pattern with respect to a threshold gain value which is sufficient to support the link budget of the wireless communication. Then, the spherical coverage can be quantified by the coverage efficiency which is defined as the ratio between the total covered solid angles and the whole surrounding sphere, i.e., 4π (see Fig. 2). The total scan pattern

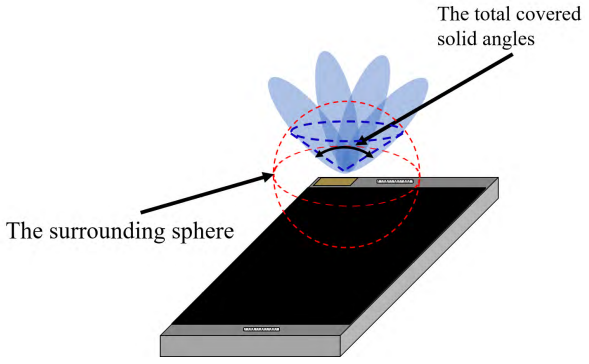

FIGURE 2. Illustration of the total covered solid angles and the surrounding sphere.

and coverage efficiency have been used recent publications in [8], [9], [14], and [15] to evaluate the spherical coverage.

The coverage efficiency is a useful parameter to evaluate the spherical coverage in terms of antenna gain. However, in a wireless system, the spherical coverage of a UE cannot be determined by only the antenna gain but also the transmitted power/receive sensitivity and the transmission losses in the radio frequency (RF) chain (e.g., the insertion loss of phase shifters). In the 3GPP specification Release 15 (Rel-15), the uplink spherical coverage of a UE is specified by the CDF of EIRP at FR2 [2], and EIRP is related to the RF performance of the transceiver chain and the array gain.

At this moment, very few publications that discuss the spherical coverage of mmWave UE with the CDF of EIRP can be found. Therefore, it motivates us to study on the 3GPP specification on spherical coverage and carry out a comprehensive investigation of the spherical coverage performance of UEs with smartphone form factors.

The major contribution of the paper can be concluded into three aspects: First, the importance of spherical coverage on the 5G mmWave mobile handsets is addressed. Second, methodologies of evaluating the UE's spherical coverage, especially the specification from the 3GPP are reviewed in the paper. Third, the spherical coverage of UEs with typical smartphone form factors is analyzed comprehensively. The analysis is not only limited to the antenna system itself but also include the phone form factors and user body effect.

The paper is organized as follows: in Section II, the importance of spherical coverage on mobile UEs is addressed with channel simulations, and the spherical coverage specifications from 3GPP will be introduced. In Section III, the spherical coverage of UEs with smartphone form factor is analyzed with different phone cover materials, array system topologies as well as different combinations of phone form factors. The user's body effect on the spherical coverage is then presented In Section IV, the corresponding influence on the downlink signal strength is illustrated with ray-tracing simulations in an urban environment. Finally, a conclusion that summarizes the main results of this paper is provided, which also includes future research directions. The antenna simulations in the paper are carried out by CST 2018.

II. CHARACTERIZATION OF THE SPHERICAL COVERAGE OF mmWave ARRAY SYSTEMS IN 5G UE

A. THE IMPORTANCE OF UE's SPHERICAL COVERAGE IN CELLULAR COMMUNICATIONS

The spherical coverage of a UE is a critical parameter for mobile communication systems, as the angle of incoming signals and the orientation of the UE will be random. In mmWave frequencies, the spherical coverage is going to be particularly critical as the channel is expected to be sparser.

In order to illustrate the importance of UE's spherical coverage, the downlink simulations with the 3GPP urban microcell (UMi) channel is carried out at 28 GHz, where the simulator is partially adopted from QuaDRiGa [17].

The simulated UMi channel model has an inter-cell distance of 200 m, which is a reasonable dimension for 5G mmWave cells (Fig. 3(a)). The simulation setups are adopted from the channel calibration model for the 3D-UMi-street Canyon case in Tab.7.8-2 in TR. 38.901 [18], except the UE antenna configurations: Two antenna array configurations in the same UE model are compared in this simulation (Fig. 3(b)): configuration 1 is with a 2 × 2 patch array which has a half wavelength inter-element distance at 28 GHz. Configuration 2 has two identical 2 × 2 patch arrays which face to the front and back side of the UE, respectively. The CDFs of their received signal-to-interference ratio (SIR) are plotted in Fig. 3(c). Since UE configuration 2 owns a double sides antenna topology, it is obvious that it has larger spherical coverage than the UE configuration 1. Consequently, the UE configurations 2 shows 4.5 dB gain at CDF = 50% comparing to configuration 1. Therefore, a mobile handset with larger spherical coverage can remain in a higher average SIR and be more robust to the rapidly changed mobile communication channels.

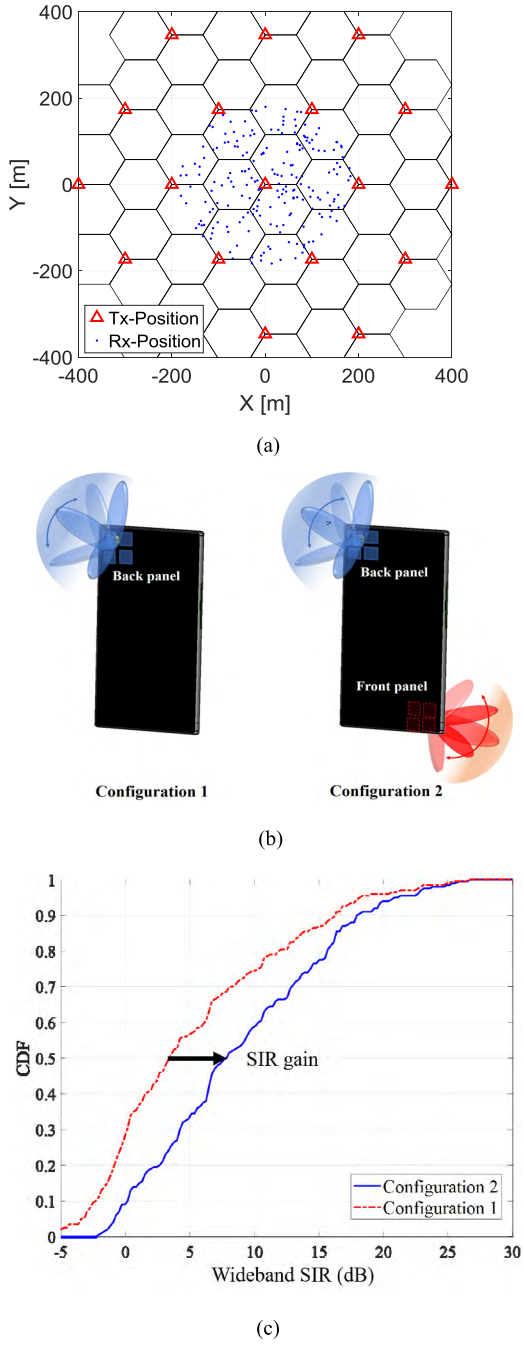

FIGURE 3. (a) The illustration of the UMi simulation. (b) The illustration of UE configuration 1 and 2 in the UMi simulation. (c) Received SINR of UEs in the 3GPP 3D-UMi channel with UE configurations 1 and 2 at 28 GHz.

B. THE 3GPP SPECIFICATION ON SPHERICAL COVERAGE FOR MOBILE HandsetType UE

In the latest and also the first 3GPP 5G specification, the uplink spherical coverage of UE is evaluated by the CDF of EIRP in FR2 [2]. EIRP is the measure of power in a specific direction, including the transmitted power, the transmission loss in the RF chain, implementation loss, the array gain and so on. The spherical coverage of a mobile handset with a linear array is illustrated in Fig. 4. The CDF of a UE's EIRP can be calculated through Eq. 1, where the right-hand side of Eq. 1 represents the probability that the measured $EIRP(\theta, \varphi)$ of the device under test (dut) takes on a value less than or equal to a threshold $EIRP$ value. The UE under the test needs to generate the transmitted beam, and also needs to support a beam-lock mode that can remain the beam during each measurement period [19].

$$CDF(EIRP) = P(EIRP_{dut}(\theta, \varphi) \leq EIRP) \tag{1}$$

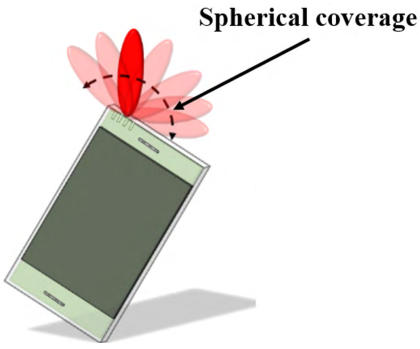

FIGURE 4. Spherical coverage of a mobile handset UE with a limited number of beams.

The EIRP value at CDF = 0% indicates the minimum EIRP level when isotropic spherical coverage is achieved, and the value when CDF = 100% shows the peak EIRP value of the array system. There are four power classes defined in FR2 in the 3GPP specification so far, and the mobile handset type UE, e.g., a smartphone, is categorized as power class 3 (PC 3). For PC3, Both the peak EIRP value and the spherical coverage performance are essential. The peak EIRP value represents the beam forming capability of UE, which is measured by the EIRP value at CDF = 100%. Therefore, the requirement is satisfied if the UE could exceed the limitation in one direction. Moreover, the requirement of spherical coverage of PC3 is specified at CDF = 50% rather

than 0% due to the compromise for practical constraints. The minimum EIRP requirements at CDF = 100 % and 50 % for PC3 are shown in Table. 2: The peak EIRP (CDF = 100%) needs to reach 22.4 dBm at frequency bands below 30 GHz (n257, n258, and n261) and 20.6 dBm at the frequency band above 37 GHz (n260). At CDF = 50%, the minimum EIRP that a mobile handset type UE needs to meet is 11.5 dBm and 8 dBm for frequency bands below 30 GHz and above 37 GHz, respectively.

TABLE 2. UE minimum peak EIRP and spherical coverage for power class 3 [2].

NR band	Min Peak EIRP (dBm)	Min EIRP at 50% CDF (dBm)
n257	22.4	11.5
n258	22.4	11.5
n260	20.6	8
n261	22.4	11.5

In addition to the absolute EIRP values, the difference between the EIRP value at CDF = 100 % and CDF = 50 % is critical as well. The difference determines the profile of the CDF curve, which is highly related to the antenna array designs in a mobile handset. An ideal antenna system with isotropic spherical coverage will have 0 dB difference, but a highly directional antenna system with limited beam-steering ability have to face a large gap between the two values. For PC 3, the difference equals to 10.9 dB at frequency bands below 30 GHz and 12.6 dB at the frequency band above 37 GHz. In order to minimize the transmitted power level that needed to meet the specification of spherical coverage For PC3 UE, it will be optimal if the difference of EIRP value at CDF = 100 % and CDF = 50% to be minimized if the peak gain is high enough, which requires the UE can transmit stable power through a large scanning angle.

The peak EIRP value of an antenna array can be affected by multiple factors, e.g., the number of elements, the output power from the power amplifier, implementation loss when the antenna is integrated into a device. Though 3GPP will not limit the practical implementation of array designs for UEs, the current peak EIRP requirement from the 3GPP assumes that each mm-Wave array panel/module is composed by a four-element antenna array [20]. Moreover, the requirement of spherical coverage (EIRP at CDF = 50 %) is based on a compromised EIRP value between a single antenna panel (e.g. configuration 1 in Fig. 3(b)) and two combined antenna panels which face different directions (e.g. configuration 2 in Fig. 3(b)) [21], [22].

It is also worthy to mention that the current specification is only applicable for UEs which support single band in FR2, the requirement of spherical coverage for UEs that support multi-bands is currently still under study.

III. THE SPHERICAL COVERAGE ANALYSIS OF mmWave MOBILE HANDSET UE WITH INTEGRATION LIMITATIONS

An antenna array in a mobile handset can be surrounded by a complicated electromagnetic environment, which will distort radiation patterns and the spherical coverage (see Fig. 5). In the latest trend of smartphone designs, metal bezels and glass made front/back covers are popularly used. Those metal structures and high permittivity materials will be highly unfavorable for integrating antenna modules at the mmWave frequency.

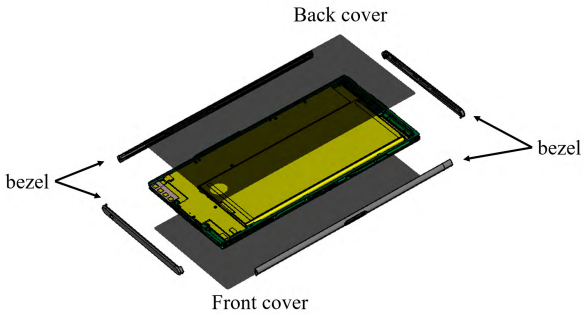

FIGURE 5. An example of a mobile handset with the smartphone form factor.

A. EIRP OF mmWave UE WITH INTEGRATION DISTORTION ON RADIATION PATTERN

Due to the decreasing thickness of smartphones nowadays, the front and back covers can be very close to the antenna modules. Therefore, the performance of antenna arrays will be particularly sensitive to the choice of the cover's material. A group of measurements at 28 GHz on the beam scanning pattern of an integrated patch array have been carried out at Aalborg University in Denmark, to investigate the impact from back cover materials of a prototype with a simplified smartphone house (only with a phone case and a ground plane). In the measurements, radiation patterns of an 8 × 1 linear patch array are measured without the back cover, with a plastic back cover as well as with a glass made back cover at 28 GHz, respectively. The patch antenna is designed on Rogers 4350B substrate ($\varepsilon r = 3.48$) with 0.468 mm thickness, and the dimension of each patch element is 2.2 mm × 2.4 mm, the interelement distance is designed to be half wavelength at 28 GHz. The back covers are placed 2 mm above the antenna array during the measurements. The impedance matching of the array remains stable with different types of back cover. The mockup of the antenna array and the prototype with the simplified smartphone house are shown in Fig. 6(a). The radiation pattern of the proposed array is steered by a digitally controlled phase shift circuit which is integrated on the back side of the antenna board.

The electromagnetic property of the back covers is critical for understanding their impact at mmWave frequency range, and thus it is characterized here. The permittivity of the plastic back cover and the glass back cover is measured by the SPEAG DAK system (see Fig. 6(b)) in Aalborg University. The permittivity of the plastic back cover equals to 2.7 with the loss tangent around 0.004 at 28 GHz, and the permittivity of the glass back cover is nearly 6 with the loss tangent around 0.028 at 28 GHz.

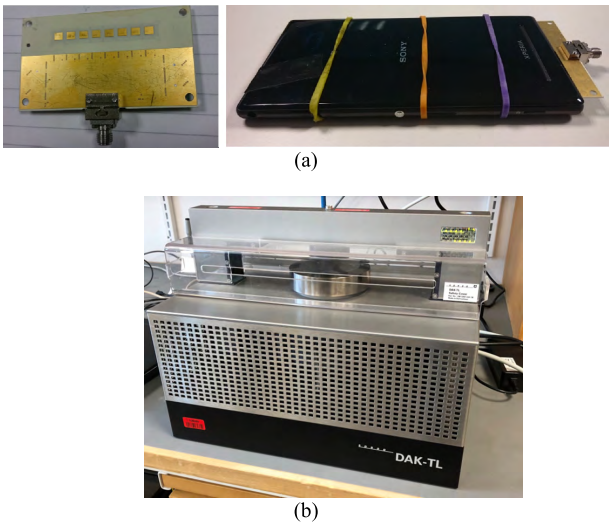

FIGURE 6. (a) A linear 8 × 1 phased array, and it is installed in a prototype. (b) Speag DAK material measurement system.

The 3D radiation patterns are measured with two beam steering angles: the first steering angle is when the beam towards the reference bore-sight of the phone (all the input phase equal to 0°), and the second steering angle is when the beam is steered to be 60° bias from the bore-sight of the phone (146° progressive phase shift). The normalized radiation patterns are shown in Fig. 7 and Fig. 8. It can be observed that the effect of the back cover on the beam steering pattern does not only depend on the material but also depend on the steering angle of the beam pattern. In Fig. 7, the beam pattern with zero phase shift (reference bore-sight) remains stable through all measurements regardless of the choice of back cover material. However, when the beam is tilted to 60° bias from bore-sight, the beam pattern is changed more prominent by the back cover: much higher sidelobes and back radiations can be observed, especially when the glass back cover is placed in front of the patch array as shown in Fig.8(c).

The 3D radiation patterns are measured with two beam steering angles: the first steering angle is when the beam towards the reference bore-sight of the phone (all the input phase equal to 0°), and the second steering angle is when the beam is steered to be 60° bias from the bore-sight of the phone (146° progressive phase shift). The normalized radiation patterns are shown in Fig. 7 and Fig. 8. It can be observed that the effect of the back cover on the beam steering pattern does not only depend on the material but also depend on the steering angle of the beam pattern. In Fig. 7, the beam pattern with zero phase shift (reference bore-sight) remains stable through all measurements regardless of the choice of back cover material. However, when the beam is tilted to 60° bias from bore-sight, the beam pattern is changed more prominent by the back cover: much higher sidelobes and back radiations can be observed, especially when the glass back cover is placed in front of the patch array as shown in Fig.8(c).

To understand the phenomenon observed above, current distributions of the proposed prototype are simulated at

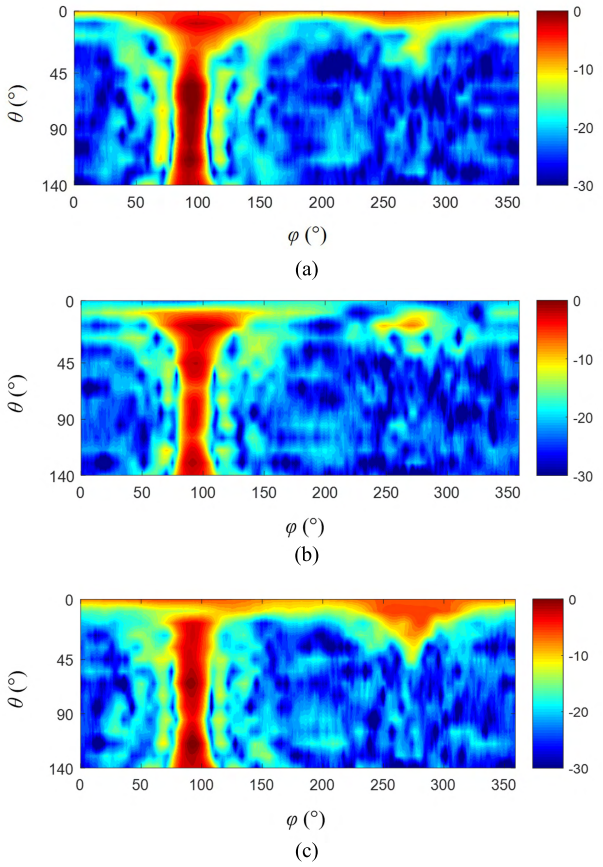

FIGURE 7. Normalized array pattern of the linear patch array to bore-sight of the phone (a) without the back cover, (b) in a phone house with a plastic back cover and (c) in a phone house with glass back cover.

28 GHz with and without the glass back cover (Fig. 9). The permittivity of the glass back cover is based on our measurement data that mentioned previously. It can be observed that a stronger current on the ground plane since the high permittivity material can guide the surface wave to propagate along the ground plane. The surface current will be diffracted when it reaches the edge of the ground plane and start to radiate into far-field. Therefore, it will interfere with the radiation from the antenna array and cause an unstable radiation pattern over different beam steering angle. The accuracy of the simulation above is verified by comparing the simulated far-field radiation patterns with the measurement results, which is shown in Fig. 9(c)-(f). It can be observed that the simulated patterns and measured patterns are similar, and the same phenomena on the far field (higher sidelobe and back radiation) can be observed when the glass back cover is introduced, which verify the validation of above simulations. A detailed analysis of the surface current in mobile handsets and its effects on spherical coverage of antenna array can be found in [23].

Based on the analysis above, the diffractions of surface current will distort the radiation pattern of antenna arrays and lead to stronger sidelobes. In a communication system, stronger sidelobes may imply potential threaten to neighbor UEs and BSs, which cause a higher interference in the system. On the other hand, stronger sidelobes may also enlarge the

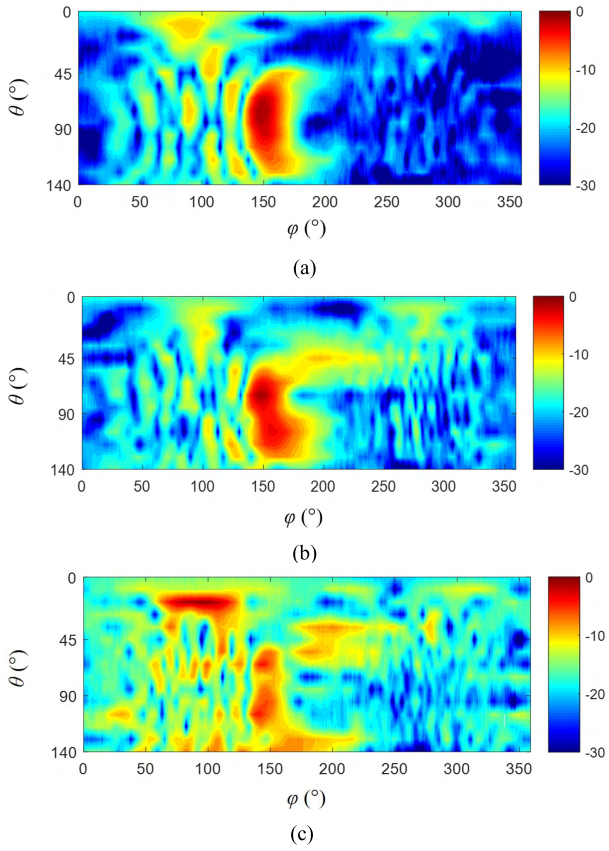

FIGURE 8. Normalized array pattern of the linear patch array to 60° bias from the bore-sight of the phone (a) without phone house, (b) in a phone house with a plastic back cover and (c) in a phone house with a glass back cover.

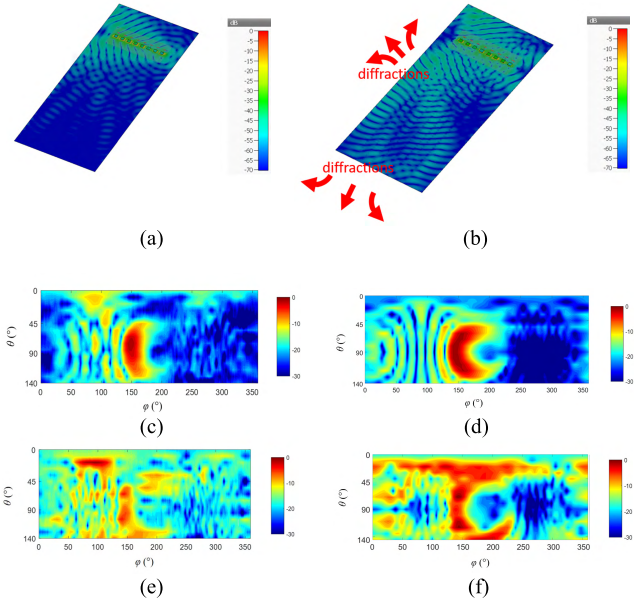

FIGURE 9. Normalized current distribution for an 8 × 1 array in a mobile phone size chassis (a) without the glass back cover and (b) with the glass back cover when the array pattern is steered to 60° bias from the bore-sight of the ground plane at 28 GHz. Comparison of the corresponding (c) measured and (d) simulated radiation pattern without the glass back cover. Comparison of the corresponding (c) measured and (d) simulated radiation pattern with the glass back cover.

spherical coverage of the UE, since the solid angles that out of main beam scanning range might be covered by sidelobes. The overall influence of sidelobes on the mmWave communication system needs to be further investigated more comprehensively.

In addition to the back cover, the existence of metal bezels around a mobile handset will cause troubles for the performance of integrated mmWave antenna arrays as well. The metal bezel will naturally block the radiation from edge mounted end-fire antenna arrays. Antenna designs to overcome this issue has been recently addressed in [24] and [25]. Moreover, the electronics inside the mobile handset will also impact the radiation and the spherical coverage of the integrated antenna system. Those issues are critical for integrating the antenna module for future 5G UEs, which will need further analysis and more advanced technologies to compromise.

B. EIRP OF MOBILE HANDSET UE WITH DIFFERENT ANTENNA TOPOLOGIES

A planar antenna array intrinsically has a quasi-hemisphere spatial coverage. Therefore, an isotropic spherical coverage can only be achieved by placing multiple antenna modules on different side/edge of a mobile handset in a switched diversity manner.

In order to provide a comprehensive evaluation on the spherical coverage of mobile handset type UEs, a computer-aided design (CAD) model of a device with smartphone form factor will be used in the simulations of sections III.B and III.C. The simulation model has been illustrated in Fig. 5, and the electronic components inside the phone, e.g., battery, speaker, connectors, are simplified as metal objects.

The impact on the spherical coverage from the number and the placement of antenna array panels in a device with smartphone form factor is firstly illustrated with three array topologies at 28 GHz (see Fig. 10 (a)): In configuration 1, a single 4 × 1 linear patch array is placed on the back side of the phone chassis. The inter-element distance is designed to be half wavelength at 28 GHz; the patch element is 2.5 mm × 3mm on a 0.3mm thick Rogers 4003c substrate ($\varepsilon r = 3.38$). In configuration 2, two 4 × 1 linear patch arrays are placed on the same side (back) of the ground plane, where one is on the top, and the other is on the bottom of the device. In the third configuration, one 4 × 1 patch antenna array is placed on the back side of the ground plane, but the other one is placed on the front side of the device (display side). For the sake of simplicity, only seven beams of each antenna array are used in the calculation of the CDF of EIRP. Each beam is generated by a progressive phase shift scheme, and the corresponding phase shift value is 0°, ±45°, ±90°, and ±135°.). Both front and back side of the model is covered by glass in the simulations, and the edge is surrounded by the metal bezel.

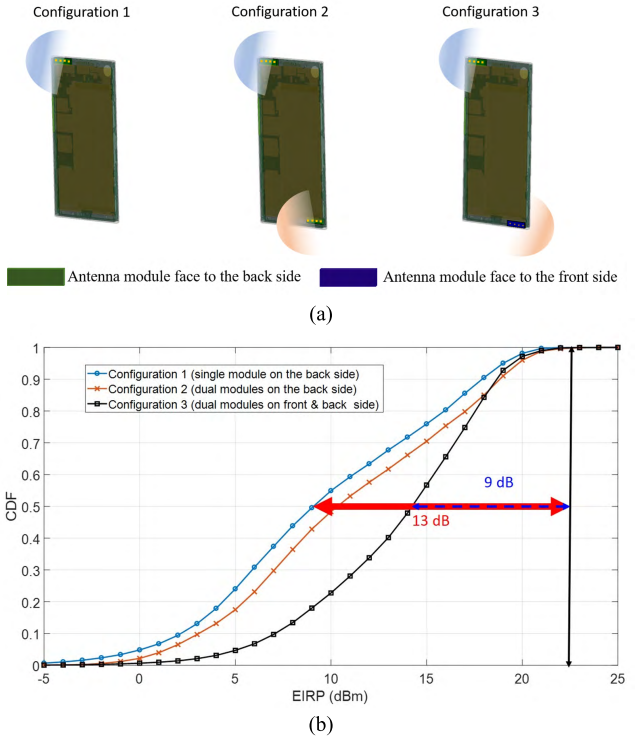

FIGURE 10. (a) Simulation models of three antenna topology configurations in a mobile device with the smartphone form factor. (b) The spherical coverage of three antenna model configurations in a mobile device with smartphone form factor at 28 GHz (total accepted power = 10 dBm).

The simulated EIRP are plotted in Fig. 10(b). The total accepted power into the antenna port is set to be 10 dBm in simulations, such that peak EIRP value is normalized to be 22.4 dBm as required by 3GPP at 28 GHz. From Fig. 10(b), it can be first observed that the peak EIRP values are aligned through three configurations, which is reasonable since the same antenna array on each panel is used here. However, as we mentioned in section II, the current 3GPP specification on the spherical coverage is compromised between the values from the single side array topology and the double side array topology. Therefore, it will be more challenging to meet the 3GPP requirement on spherical coverage for configuration 1 and configuration 2: higher conducted power will be needed to satisfy the requirement of EIRP for spherical coverage (CDF = 50%) than the peak value (CDF = 100%) with the potential risk of violating the maximum allowed TRP limit. In addition, the spatial diversity gain in configuration 2 shows a minimal improvement on the spherical coverage of the UE since both antenna arrays face to the same side of the phone. On the other hand, when multiple arrays placed towards different sides of the device, the 3GPP specification on spherical coverage will be relaxed to be met. As a result, the first two configurations (1 and 2) will require at least 13 dBm and 11.5 dBm accepted power in order to meet the 3GPP specification at both CDF = 100% and 50%, but it will only require 10 dBm accepted power for configuration 3 to meet those values.

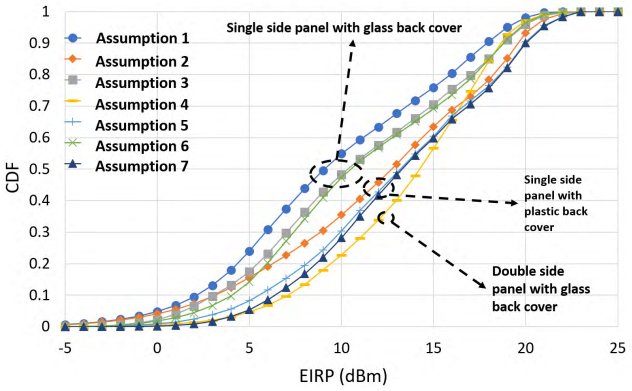

FIGURE 11. Spherical coverage of seven different form factor of mobile handset designs at 28 GHz (total accepted power = 10 dBm).

C. EIRP OF mmWave MOBILE HANDSET UE WITH DIFFERENT FORM FACTORS

The impact due to the integration distortion and array topologies have been discussed in III. A and III. B, respectively. It can be learned that both the choice of the device form materials and the array topology will impact the spherical coverage of a UE. In practical, there needs to be a tradeoff between the optimal antenna array topology and the phone form factors. For example, a smartphone with a display which fully occupies the front side of the phone can prevent or at least increase the difficulty in placing an antenna array that radiates toward to the front side of the phone. Therefore, it requires a compromised design which can balance between the optimal antenna system and the phone form factor, in order to ensure that the device can meet the 3GPP specification.

In order to provide a comprehensive study on the spherical coverage performance in different phone form factors (e.g., back cover material and display portion), multiple simulations are carried out here, and the phone form factors are according to the reference assumptions in 3GPP way forward (WF) on EIRP CDF for spherical coverage study [26]. Each antenna panel is modeled as a 4 × 1 linear patch array which is the same as illustrated in Fig. 10. The same simulation model as in III.B is used. All simulated phone form factor combinations are shown in Tab. 3.

TABLE 3. Simulations assumption for different form factor combinations of mobile handset UE.

Simulation Assumption	1	2	3	4	5	6	7
Display	Full	Full	Full	Partial	Full	Full	Full
Number of antenna panels on front side	1	1	2	1	2	3	3
Number of antenna panels on back side	0	0	0	1	0	0	0
Phone frame material	Metal	Metal	Metal	Metal	Metal	Metal	Metal
Back cover material	Glass	Plastic	Glass	Glass	Plastic	Glass	Plastic
Front cover material	Glass	Glass	Glass	Glass	Glass	Glass	Glass

The simulation results are shown in Fig. 11, where the accepted power is normalized to 10 dBm. It can be observed that though the peak EIRP is very similar through all simulations, the EIRP value at CDF = 50% can vary dramatically. With a phone form factor with full display, the antenna array may only be allowed to be placed on the back side of the device here. Consequently, the spherical coverage of such a device will be profoundly affected by choice of back cover material. On the other hand, with double side antenna panels, the conditions to meet the EIRP specification of 3GPP is better, and thus higher degrees of freedom on the phone designs are granted. More analysis has also been presented in [27].

To verify the accuracy of the simulation setup that has been used in previous simulations, we compare the simulated CDF curve at 28 GHz from the device model with the measurement result of an evaluation prototype (smartphone form factor) which includes all components such as, e.g., display and battery. In the evaluation prototype, the back cover and bezel are composing of plastic, where the front side is covered by full glass. For this comparison, the mmWave antenna system in the prototype is composed of two 2 × 2 patch arrays which face to the front and the back side of the phone, respectively. Though the array topology is slightly modified, the structure of the device model and the simulation setup is identical with previous simulations. The simulated and measured CDF of EIRP are plotted in Fig. 12: The difference between the simulated and measured EIRP at CDF = 50% is only about 0.5 dB, which verify the accuracy of the simulation setup.

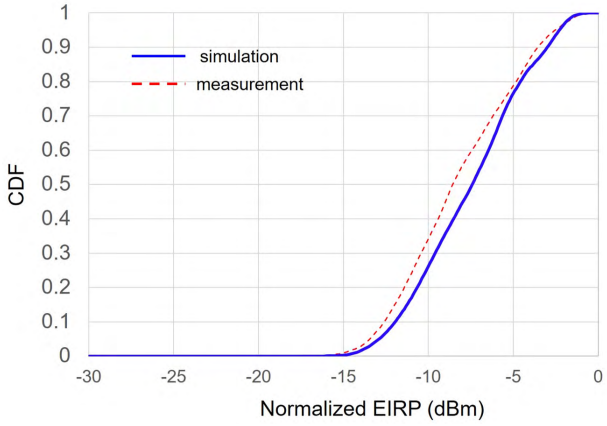

FIGURE 12. Comparison of the measured and simulated CDF of EIRP of the evaluation prototype with a smartphone form factor.

IV. THE SPHERICAL COVERAGE ANALYSIS OF mmWave UE SYSTEMS WITH A USER BODY BLOCKAGE

In real life, the spherical coverage of a UE will also be influenced by the presence of the user. Though this limitation is not considered in the 3GPP specification currently, its impact will be unneglectable in mmWave bands. It has been observed in [28]–[32] that the presence of user body will cause a pounced shadowing region in the surrounding spherical of UE arrays, due to the increased transmission and diffraction loss of the human body at higher frequencies.

To better understand the influence of the user blockage on spherical coverage, the total scan pattern [16] of a 4 × 1 linear array on top of a mobile phone mockup is measured with a real user in a standing position (see Fig. 13, the antenna is illustrated as "edge mounted array (top)" in Fig. 14(a)). The dimension of the element is about 4 mm × 0.8 mm, and the inter-element distance is about half wavelength at 28 GHz. The measurements were also carried out in an anechoic chamber at Aalborg University, Denmark. The shadowing of the human body shape can be clearly observed, and the loss in the deep shadowing region is about 30 dB.

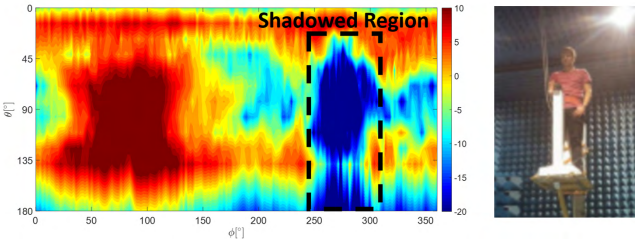

FIGURE 13. The total scan pattern with a user body blockage.

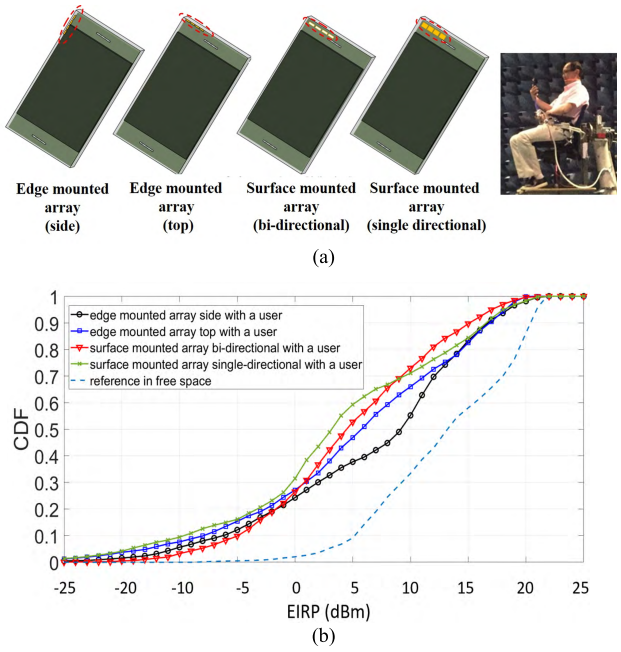

FIGURE 14. (a) User body blockage for the antenna arrays with four element designs (within the red line). (b) The spherical coverage with user body blockage for the antenna arrays. (total accepted power = 10 dBm).

For further understand the blockage effect of the user's body on UE's EIRP, the radiation pattern of four 4 × 1 linear arrays (with four different element designs) are measured with a real user in sitting position, which is illustrated in Fig. 14(a). The four element designs radiate towards the left side of the handset, the top side of the handset, the front side of the handset and both front and back side

of the handset, respectively. The four arrays have the same half wavelength inter-element distance at 28 GHz but with complementary radiation patterns, which composes a solid basis for a benchmark comparison. The CDFs of EIRP with user body blockage for the antenna sub-arrays are shown in Fig. 14(b), the spherical coverage is calculated with seven beams as in the previous section, where the beam pattern of each array is synthesized through a single embedded element pattern to avoid the phase drift between different elements in the measurements. The accepted power is set to be 10 dBm here as well, to normalize the peak EIRP to be the 22.4 dBm. It can be observed that the peak EIRP value remains almost unchanged through all the results. However, EIRP values at CDF = 50 % drop about 5-10 dB compared to the reference case that without the user. Meanwhile, the difference among the proposed element designs is relatively small at CDF = 50% when the user is holding the prototype.

Due to the loss of spherical coverage, the received signal strength in a real-life propagation environment is expected to be influenced as well. A ray-tracing simulation at 28 GHz is carried out, where an urban scenario model based on the environment in Kista, Stockholm, Sweden is simulated, which is shown in Fig. 15(a). The ray-tracing simulations are carried out by Wireless Insite (v.2.8), and the detail information and discussion of this ray-tracing model can be found in [32]. The downlink signal strength (RSS) of a user which is placed about 150 m away from the BS is simulated: The propagation

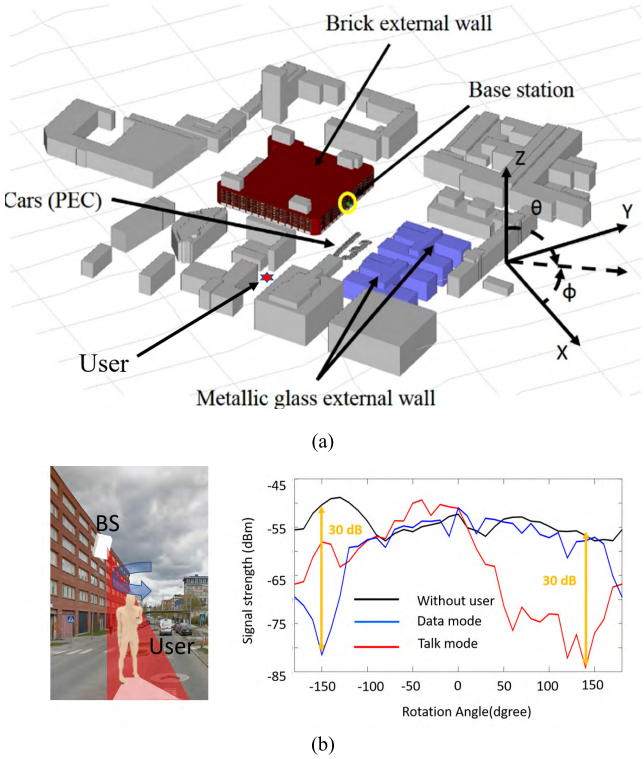

FIGURE 15. (a) Ray-tracing simulation model at Kista, Stockholm, Sweden. (b) The received signal strength with rotated orientations the user at 28 GHz.

environment is under Line-of-Sight (LoS) with reflections from the buildings and the ground. The measured embedded radiation patterns with the real user are used on the user side [32]. The orientation of the user is rotated 10 degrees for every snapshot, and the received signal strength when the user is absent (i.e., no user body blockage), when the user holds the UE in data mode and when the user holds the UE in talk mode [33] are shown in Fig. 15(b): A dramatic fluctuation of the RSS can be observed, where the signal strength can drop 30 dB due to the user body blockage.

In [30], the user shadowing (or blockage) of 12 users has also been measured at 28 GHz. It finds out that the power within the shadowed region may have over 10 dB difference between individuals. The power in the shadowed region can be impacted by many factors such as the user's height, weight, skin property, clothes and so on. It will increase the uncertainty of spherical coverage for different individuals in real life.

V. CONCLUSION

In this paper, the characterization of spherical coverage of mmWave 5G UE has been discussed. Due to the randomness of the mobile wireless channel, it is essential that a mobile device can achieve a large spherical coverage in order to maintain a stable coverage of the cellular system. System simulations have been presented to illustrate the improvement in downlink SIR of a cellular system due to a better spherical coverage of UE at 28 GHz.

Based on the first 5G standard 3GPP Rel-15, The CDF of EIRP has been used to evaluate the spherical coverage of a 5G UE in FR2. The CDF of EIRP is an efficient tool to characterize the spherical coverage performance of the whole UE array system including the transmitted power, losses in beamforming networks, the array gain, user blockage, and all the other losses in the UE system.

Due to the increased operating frequency, the array performance will be more sensitive to the objects nearby in mmWave range than at sub-6GHz, especially to high-permittivity materials and metal structures around. Therefore, those materials must be carefully selected to ensure that the spherical coverage of the UE can be acceptable. Moreover, the phone form factors will imply additional constraints on the choice of array topologies, which introduces additional challenges to the antenna system design and integration for the mobile handset.

User body blockage is another unneglectable factor that will limit the spherical coverage of mobile handset type UE. The dramatic shadowing loss in the mmWave frequency range from human body will cause degradation on the link budget of the mobile communication, and its random orientation can bring an additional variation on the transmitted and received signal strength of the UE. This factor must be considered in priority to the network planning, in order to ensure a stable operation of the 5G network.

In addition to the major issues that have been analyzed above, other factors, e.g., pre-coding errors,

measurement uncertainties and limitations on the human exposure [34]–[37] will also impact the spherical coverage of UEs. Moreover, the spherical coverage of UE's receiver performance is still under discussion [38]. More contributions will be needed to complete the characterization of the UE spherical coverage in the future.

REFERENCES

[1] Z. Pi and F. Khan, "An introduction to millimeter-wave mobile broadband systems," *IEEE Commun. Mag.*, vol. 49, no. 6, pp. 101–107, Jun. 2011.

[2] *User Equipment (UE) Radio Transmission and Reception; Part 2: Range 2 Standalone (Release 15)*, document TS38.101-2 v15.0.0, Jun. 2018.

[3] T. S. Rappaport *et al.*, "Millimeter wave mobile communications for 5G cellular: It will work!" *IEEE Access*, vol. 1, pp. 335–349, 2013.

[4] I. Rodriguez *et al.*, "Analysis of 38 GHz mmWave propagation characteristics of urban scenarios," in *Proc. 21th Eur. Wireless Conf.*, Budapest, Hungary, 2015, pp. 1–8.

[5] W. Hong, K.-H. Baek, Y. Lee, Y. Kim, and S.-T. Ko, "Study and prototyping of practically large-scale mmWave antenna systems for 5G cellular devices," *IEEE Commun. Mag.*, vol. 52, no. 9, pp. 63–69, Sep. 2014.

[6] W. Hong, K.-H. Baek, and S. Ko, "Millimeter-wave 5G antennas for smartphones: Overview and experimental demonstration," *IEEE Trans. Antennas Propag.*, vol. 65, no. 12, pp. 6250–6261, Dec. 2017.

[7] S.-J. Park, D.-H. Shin, and S.-O. Park, "Low side-lobe substrate-integrated-waveguide antenna array using broadband unequal feeding network for millimeter-wave handset device," *IEEE Trans. Antennas Propag.*, vol. 64, no. 3, pp. 923–932, Mar. 2016.

[8] N. Ojaroudiparchin, M. Shen, S. Zhang, and G. F. Pedersen, "A switchable 3-D-coverage-phased array antenna package for 5G mobile terminals," *IEEE Antenna Wireless Propag. Lett.*, vol. 15, pp. 1747–1750, 2016.

[9] S. Zhang, X. Chen, I. Syrytsin, and G. F. Pedersen, "A planar switchable 3-D-coverage phased array antenna and its user effects for 28-GHz mobile terminal applications," *IEEE Trans. Antennas Propag.*, vol. 65, no. 12, pp. 6413–6421, Dec. 2017.

[10] J. Park, S. Y. Lee, Y. Kim, J. Lee, and W. Hong, "Hybrid antenna module concept for 28 GHz 5G beamsteering cellular devices," in *Proc. IEEE MTT-S Int. Microw. Workshop Ser., 5G Hardw. Syst. Technol. (IMWS-5G)*, Aug. 2018, pp. 1–3.

[11] M. Stanley, Y. Huang, H. Wang, H. Zhou, A. Alieldin, and S. Joseph, "A capacitive coupled patch antenna array with high gain and wide coverage for 5G smartphone applications," *IEEE Access*, vol. 6, pp. 41942–41954, 2018.

[12] Y. Yashchyshyn *et al.*, "28 GHz switched-beam antenna based on S-PIN diodes for 5G mobile communications," *IEEE Antennas Wireless Propagat. Lett.*, vol. 17, no. 2, pp. 225–228, Feb. 2018.

[13] Q.-L. Yang, Y.-L. Ban, K. Kang, C.-Y.-D. Sim, and G. Wu, "SIW multibeam array for 5G mobile devices," *IEEE Access*, vol. 4, pp. 2788–2796, 2016.

[14] K. R. Mahmoud and A. M. Montaser, "Design of dual-band circularly polarised array antenna package for 5G mobile terminals with beam-steering capabilities," *IET Microw., Antennas Propag.*, vol. 12, no. 1, pp. 29–39, 2017.

[15] I. Syrytsin, S. Zhang, G. F. Pedersen, and Z. Ying, "User effects on the circular polarization of 5G mobile terminal antennas," *IEEE Trans. Antennas Propag.*, vol. 66, no. 9, pp. 4906–4911, Sep. 2018.

[16] J. Helander, K. Zhao, Z. Ying, and D. Sjöberg, "Performance analysis of millimeter-wave phased array antennas in cellular handsets," *IEEE Antennas Wireless Propag. Lett.*, vol. 15, pp. 504–507, Mar. 2016.

[17] S. Jaeckel, L. Raschkowski, K. Börner, and L. Thiele, "QuaDRiGa: A 3-D multi-cell channel model with time evolution for enabling virtual field trials," *IEEE Trans. Antennas Propag.*, vol. 62, no. 6, pp. 3242–3256, Jun. 2014.

[18] *Study on Channel Model for Frequencies From 0.5 to 100 GHz (Release 15), V15.0.0*, document 3GPP TR 38.901, Jun. 2018.

[19] *Study on Test Methods for New Radio, V2.3.0*, document 3GPP TR 38.810, Aug. 2018.

[20] *WF on Pulse Shaping and Power Class FR2*, document R4-1714373, 3GPP TSG-RAN WG4 Meeting #85, Reno, NV, USA, Nov. 2017.

[21] *WF for Spherical Coverage for FR2*, document R4-1808198, 3GPP TSG RAN WG4 Meeting #87, Busan, South Korea, May 2018.

[22] *Proposals for Concluding the Spherical Coverage Requirement for FR2 Handheld UEs*, document R4-1808173, 3GPP TSG RAN WG4 Meeting #87, Busan, South Korea, May 2018.

[23] B. Xu *et al.*, "Radiation performance analysis of 28 GHz antennas integrated in 5G mobile terminal housing," *IEEE Access*, vol. 6, pp. 48088–48101, 2018.

[24] B. Yu, K. Yang, C.-Y.-D. Sim, and G. Yang, "A novel 28 GHz beam steering array for 5G mobile device with metallic casing application," *IEEE Trans. Antennas Propag.*, vol. 66, no. 1, pp. 462–466, Jan. 2018.

[25] R. Rodriguez-Cano, S. Zhang, K. Zhao, and G. Pedersen, "Reduction of main beam-blockage in an integrated 5G array with a metal-frame antenna," *IEEE Trans. Antennas Propag.*, to be published.

[26] *WF on Spherical Coverage in FR2*, document R4-1714455, Samsung, Apple, LGE, Intel, Oppo, Xiaomi, Vivo, MediaTek, 3GPP RAN4 Nov. 2017, vol. 85.

[27] *UE Spherical Coverage at mmWave 28GHz*, document R4-1805321, Sony, Ericsson, 3GPP TSG-RAN WG4 Meeting #86Bis, Melbourne, VIC, Australia, Apr. 2018.

[28] K. Zhao, J. Helander, D. Sjöberg, S. He, T. Bolin, and Z. Ying, "User body effect on phased array in user equipment for the 5G mmWave communication system," *IEEE Antennas Wireless Propag. Lett.*, vol. 16, pp. 864–867, 2017.

[29] K. Zhao *et al.*, "Channel characteristics and user body effects in an outdoor urban scenario at 15 and 28 GHz," *IEEE Trans. Antennas Propag.*, vol. 65, no. 12, pp. 6534–6548, Dec. 2017.

[30] I. Syrytsin, S. Zhang, G. F. Pedersen, K. Zhao, T. Bolin, and Z. Ying, "Statistical investigation of the user effects on mobile terminal antennas for 5G applications," *IEEE Trans. Antennas Propag.*, vol. 65, no. 12, pp. 6596–6605, Dec. 2017.

[31] I. Syrytsin, S. Zhang, and G. F. Pedersen, "User impact on phased and switch diversity arrays in 5G mobile terminals," *IEEE Access*, vol. 6, pp. 1616–1623, 2018.

[32] T. Bai and R. W. Heath, Jr., "Analysis of self-body blocking effects in millimeter wave cellular networks," in *Proc. 48th Asilomar Conf. Signals, Syst. Comput.*, Pacific Grove, CA, USA, 2014, pp. 1921–1925.

[33] *Test Plan for Wireless Device Over-the-Air Performance*, CTIA, Washington, DC, USA, Nov. 2016.

[34] B. Xu *et al.*, "Power density measurements at 15 GHz for RF EMF compliance assessments of 5G user equipment," *IEEE Trans. Antennas Propag.*, vol. 65, no. 12, pp. 6584–6595, Dec. 2017.

[35] B. Xu, M. Gustafsson, S. Shi, K. Zhao, Z. Ying, and S. He, "Radio frequency exposure compliance of multiple antennas for cellular equipment based on semidefinite relaxation," *IEEE Trans. Electromagn. Compat.*, to be published.

[36] W. He, B. Xu, M. Gustafsson, Z. Ying, and S. He, "RF compliance study of temperature elevation in human head model around 28 GHz for 5G user equipment application: Simulation analysis," *IEEE Access*, vol. 6, pp. 830–838, 2018.

[37] B. Thors, D. Colombi, Z. Ying, T. Bolin, and C. Törnevik, "Exposure to RF EMF from array antennas in 5G mobile communication equipment," *IEEE Access*, vol. 4, pp. 7469–7478, 2016.

[38] *Minute on EIS Spherical Coverage Ad Hoc*, document R4-1811522, 3GPP TSG-RAN WG4 #88, Gothenburg, Sweden, Aug. 2018.

KUN ZHAO received the B.S. degree in communication engineering from the Beijing University of Posts and Telecommunications, Beijing, China, in 2010, and the M.S. degree in wireless systems and the Ph.D. degree in electromagnetic engineering from the Royal Institute of Technology (KTH), Stockholm, Sweden, in 2012 and 2017, respectively.

He was a Visiting Researcher with the Department of Electrical and Information Technology, Lund University, Sweden. He is currently a Researcher of antenna technology and standardization with the Radio Access Lab, Sony Mobile Communications AB, Lund, Sweden. He also holds an industrial Post-doctoral position with Aalborg University, Denmark. His current research interests include millimeter-wave antenna and propagation for fifth-generation communications, multi-in multi-out antenna systems, user body interactions, and body-centric wireless communications.

SHUAI ZHANG received the B.E. degree from the University of Electronic Science and Technology of China, Chengdu, China, in 2007, and the Ph.D. degree in electromagnetic engineering from the Royal Institute of Technology (KTH), Stockholm, Sweden, in 2013. He was a Research Fellow with KTH. In 2010 and 2011, he was a Visiting Researcher with Lund University, Sweden, and also with Sony Mobile Communications AB, Sweden, respectively. In 2014, he joined Aalborg University, Denmark. He was also an External Antenna Specialist with Bang & Olufsen, Denmark, from 2016 to 2017. He is currently an Associate Professor with Aalborg University. He has co-authored over 40 articles in well-reputed international journals and holds over 14 (U.S. or WO) patents. His research interests include mobile terminal millimeter-wave antennas, biological effects, CubeSat antennas, UWB wind turbine blade deflection sensing, multi-in multi-out antenna systems, and RFID antennas.

ZULEITA HO (S'05–M'11) received the B.Eng. and M.Phil. degrees in electronic engineering (wireless communication) from The Hong Kong University of Science and Technology, in 2005 and 2007, respectively, and the Ph.D. degree in wireless communications from EURECOM and Telecom Paris, France, in 2010. In 2004, she joined the Massachusetts Institute of Technology as a Visiting Scholar. From 2011 to 2013, she was a Post-Doctorate Research Fellow with the Chair of Communications Theory, Dresden University of Technology, Germany. From 2013 to 2015, she was a Senior Engineer with Advanced Communications Laboratory, DMC Research and Development Center, Samsung Electronics, South Korea. From 2015 to 2017, she was a Senior Research Engineer with Advanced Algorithm Team, Huawei Technologies, Sweden. Since 2017, she has been a Senior Research Engineer with the Radio Access Technology Group, Research and Standardization Team, Sony Mobile Communications, Sweden.

OLOF ZANDER received the M.Sc. degree in electrical engineering and the Licentiate degree in engineering, with a focus on applied radio frequency (RF) application-specified integrated circuit (ASIC) design, from Lund University, Sweden, in 1985 and 1991, respectively. He joined Ericsson Mobile Communications, Lund, in 1992, where he involved in the RF design of mobile phones and RF ASIC design. From 1997 to 2000, he was the Technical Manager for a group of RF engineers, and from 2000 to 2007, in a similar position leading a group of RF ASIC designers. In 2007, he joined Sony-Ericsson Mobile Communications as the Project Manager for developing the RF modem subassembly used in the complete product line. Since 2012, he has been a 3GPP RAN4 Delegate.

THOMAS BOLIN received the M.Sc. degree in applied physics and electrical engineering from Linköping University, Sweden, in 1979. From 1979 to 1983, he was a Radio Frequency (RF)-Development Engineer with ITT Standard Radio & Telefon AB, Stockholm, where he focused on 1-kW HF PA and filter designs. From 1983 to 2001, he held a technical management position with Ericsson Mobile Communications, Lund, Sweden, where he involved not only in the RF and antenna product development but also in the OTA measurement technology development for mobile handsets. From 2001 to 2011, he also held a technical management position with Sony Ericsson Mobile Communications, Lund, and has been with Sony Mobile Communications, Lund, since 2011, where he is currently more devoted to antenna research and standardization. He is currently a 3GPP RAN4 Delegate. He assisted in the development of millimeter-wave antenna arrays and FEM integration (15–40 GHz) for fifth generation.

ZHINONG YING is currently a Principle Engineer of antenna technology with Access Technology Lab, Research and Technology, Sony Mobile Communication AB, Lund, Sweden. He is also a Distinguished Engineer with the whole Sony Group. He joined Ericsson AB, in 1995, where he became a Senior Specialist, in 1997, and an Expert, in 2003, in his engineering career. He has been a Guest Professor with the Joint Research Centre, Royal Institute of Technology, Sweden, and also with Zhejiang University, China, since 2001. He was a member of the Scientific Board of ACE Program (Antenna Centre of Excellent in European 6th Frame), from 2004 to 2007. He is a Senior Member of the IEEE. He served as a TPC Co-Chairman for the International Symposium on Antenna Technology, in 2007, as a session organizer for several international conferences, including IEEE APS, and as a reviewer for several academic journals.

He has authored or co-authored over 150 papers in various journals, conferences, and industry publications. He holds more than 150 patents granted and pending, in the antennas and new generation wireless network areas. His main research interests include small antennas, broad and multi-band antenna, multi-channel antenna [multi-in multi-out (MIMO)] system, antenna for body area network, antenna and propagation in fifth-generation mobile network including massive MIMO and millimeter wave, near field, and human body effects and measurement techniques. He contributed several book chapters on mobile antenna, small antenna, and MIMO antennas in *Mobile Antenna Handbook* (3rd edition) edited by H. Fujimoto and in the *Handbook of Antenna Technologies* edited by Z. N. Chen. He had contributed a lot to antenna designs and evaluation methods for the mobile industry. He also involved in the evaluation of Bluetooth technology which was invented by Ericsson. He was nominated for the President Award at Sony Ericsson, in 2004, for his innovative contributions. He received the Best Invention Award at Ericsson Mobile, in 1996, and the Key Performer Award at Sony Ericsson, in 2002. He received the Distinguish Engineer title at the Sony Group, in 2013.

GERT FRØLUND PEDERSEN was born in 1965. He received the B.Sc. and E.E. (Hons.) degrees in electrical engineering from the College of Technology in Dublin, Dublin Institute of Technology, Dublin, Ireland, in 1991, and the M.Sc.E.E. and Ph.D. degrees from Aalborg University, Aalborg, Denmark, in 1993 and 2003, respectively. He was a Consultant for the development of more than 100 antennas for mobile terminals, including the first internal antenna for mobile phones, in 1994, with lowest SAR, first internal triple-band antenna, in 1998, with low SAR and high total radiated power and total isotropic sensitivity, and lately various multiantenna systems rated as the most efficient in the market. Since 1993, he has been with Aalborg University, where he is currently a Full Professor, heading the Antennas, Propagation and Millimeter-Wave Systems Lab with 25 researchers. He is also the Head of the Doctoral School on Wireless Communication with some 40 Ph.D. students enrolled. He has worked most of the time with joint university and industry projects and has received more than $21 million in direct research funding. He is currently the Project Leader of the RANGE Project with a total budget of over $8 million, investigating high-performance centimeter/millimeter-wave antennas for fifth-generation mobile phones. He has been one of the pioneers in establishing over-the-air (OTA) measurement systems. The measurement technique is now well established for mobile terminals with single antennas, and he was chairing the various COST groups with liaison to 3GPP and CTIA for OTA test of multi-in multi-out (MIMO) terminals. He is currently involved in MIMO OTA measurement. He has published more than 500 peer-reviewed papers, six books, and 12 book chapters, and holds over 50 patents. His research interests include radio communication for mobile terminals, especially small antennas, diversity systems, propagation, and biological effects.